Efficient Computation of Power, Force, and Torque in BEM Scattering Calculations

Citation: Reid, M. T. Homer, and Steven G. Johnson. "Efficient Computation of Power, Force, and Torque in BEM Scattering Calculations." IEEE Transactions on Antennas and Propagation 63, no. 8 (August 2015): 3588–3598.

As Published: http://dx.doi.org/10.1109/tap.2015.2438393

Publisher: Institute of Electrical and Electronics Engineers (IEEE)

Persistent URL: http://hdl.handle.net/1721.1/110217

Version: Author's final manuscript: final author's manuscript post peer review, without publisher's formatting or copy editing

This article has been accepted for publication in a future issue of this journal, but has not been fully edited. Content may change prior to final publication. Citation information: DOI 10.1109/TAP.2015.2438393, IEEE Transactions on Antennas and Propagation

Efficient Computation of Power, Force, and Torque in BEM Scattering Calculations

M. T. Homer Reid and Steven G. Johnson

***Abstract*—We present concise, computationally efficient formulas for several quantities of interest—including absorbed and scattered power, optical force (radiation pressure), and torque—in scattering calculations performed using the boundary-element method (BEM) [also known as the method of moments (MoM)]. Our formulas compute the quantities of interest *directly* from the BEM surface currents with no need ever to compute the scattered electromagnetic fields. We derive our new formulas and demonstrate their effectiveness by computing power, force, and torque in a number of example geometries. Free, open-source software implementations of our formulas are available for download online [1].**

***Index terms:* Method of moments, electromagnetic propagation, extinction coefficients, nanophotonics, Casimir effect, nanosensors, force, torque**

I. Introduction

This paper presents and compares several distinct formulas for the time-average absorbed and scattered power, force (radiation pressure), and torque exerted on material bodies by incident fields. Our formulas, which are derived in the context of the frequency-domain boundary-element method [BEM, also known as the method of moments (MoM)], express powers, forces, and torques (PFTs) in terms of vector–matrix–vector products involving various matrices sandwiched between the vectors of BEM surface-current coefficients. We present the derivation of our formulas, compare their relative merits, and apply them to a number of example geometries.

The primary goal of electromagnetic scattering solvers is to compute the electric and magnetic fields in a given material geometry illuminated by given incident fields or sources. However, in many cases we are less interested in the fields themselves than in certain derived quantities obtained from them. For example, in a scattering problem we may be more interested in the total absorbed power or the total scattering cross section than in the individual fields at particular points in space [2], [3]. Similarly, for the problem of a mesoscopic structure [4], [5] or nanoparticle [6]–[8] illuminated by a laser, we may seek the force or torque exerted on the particle by the incident-field sources.

Of course, derived quantities such as power, force, and torque may always be computed *indirectly* in any scattering formalism by first computing the scattered fields and then post-processing: powers and forces/torques are obtained respectively by integrating the Poynting vector (PV) and the Maxwell stress tensor (MST) over a bounding surface surrounding the object in question, with values of the PV and MST at each surface point computed using field components obtained from the scattering solver. However, in practice the integration may be numerically badly behaved due to large cancellations from different regions of the bounding surface, requiring large numbers of cubature points to obtain accurate results. Moreover, in scattering formalisms such as the BEM—where, unlike other techniques such as the finite-difference and finite-element methods, the fields are not computed directly as part of the solution to the problem—each field evaluation required to evaluate the PV or MST integrals by numerical cubature costs extra work.

Our goal here is to consider techniques for expressing PFTs directly in terms of the surface currents that are the immediate output of the BEM solution procedure. Since the PV and MST are quadratic in the fields and the fields are linear in the currents, it follows that PFTs are quadratic in currents and may be generally expressed as bilinear products of the form

$$Q = \mathbf{c}^\dagger \mathbf{Q} \mathbf{c} \tag{1}$$

where Q is the quantity in question (a power force, or torque), $\mathbf{c}$ is the vector of surface-current coefficients (obtained, in a BEM scattering problem, by solving a linear system $\mathbf{M}\mathbf{c} = \mathbf{f}$ where $\mathbf{M}$ is the BEM matrix and the RHS vector $\mathbf{f}$ describes the incident field), and $\mathbf{Q}$ is a Q-dependent matrix. As it turns out, for a given quantity Q there are several distinct ways to write matrices $\mathbf{Q}$, each with their own merits, which we discuss and compare here.

Expressing PFTs as surface-current bilinears like (1) is not merely a matter of convenience, but is also the key to the fluctuating-surface-current (FSC) approach to numerical modeling of fluctuation-induced phenomena such as Casimir forces and radiative heat transfer [9], [10]. Indeed, in recent work [11] we have demonstrated the following correspondence: If, in a classical deterministic scattering problem, a PFT quantity Q may be expressed in the form of equation (1), then the statistical average of Q over quantum and thermal fluctuations of sources may be expressed in the form

$$\langle Q \rangle = \mathrm{Tr}\left(\mathbf{Q}\mathbf{\Sigma}\right) \tag{2}$$

where $\mathbf{Q}$ is the *same* matrix that appears in (1) and $\mathbf{\Sigma}$ is a certain temperature-dependent matrix describing source fluctuations inside bodies [11]. In this paper we are concerned with classical deterministic problems, and thus PFT formulas of the form (1); but we explore the implications of these formulas with an eye toward applying them to fluctuation phenomena through equation (2).

To date a variety a methods have been used to compute PFTs for compact bodies. For bodies of highly symmetric

M. T. Homer Reid is with the Department of Mathematics, Massachusetts Institute of Technology.

S. G. Johnson is with the Department of Mathematics, Massachusetts Institute of Technology.

This article has been accepted for publication in a future issue of this journal, but has not been fully edited. Content may change prior to final publication. Citation information: DOI 10.1109/TAP.2015.2438393, IEEE Transactions on Antennas and Propagation

shapes such as spheres or cylinders, exact results are available in analytical form (such as Mie theory for spheres) [12], [13], and these closed-form solutions may be used to compute PFTs for such bodies [14]–[17], or extended to the case of spheroidal bodies [18]. For bodies small compared to the incident wavelength ("Rayleigh particles"), PFTs may be computed using quasistatic approximations [19]–[23], while in the opposite regime (bodies large compared to the incident wavelength) the geometrical-optics approximation is available [24]–[26]. Radiation forces for nonspherical bodies have also been computed using quasi-analytical approaches (numerical methods based on analytical solutions for special geometries), including T-matrix methods [27] and discrete dipole approximations [28], Among fully numerical techniques, compact-object PFTs have been computed using finite-difference time-domain (FDTD) methods [4], [8], [29]–[31] and finite-element methods [32]–[34].

BEM techniques have been used by several authors to characterize *local* power absorption [35]–[38], and were used in Ref. 39 to compute total cross sections for scattering and absorption by a compact body. Ref. 5 employed a BEM technique to investigate the force and torque on a mesoscopic body illuminated by a laser beam, while Ref. 40 used the BEM to compute radiation forces on two-dimensional structures. In all of these BEM studies, the standard BEM approach was applied to solve for surface currents, after which the surface currents were used to compute scattered fields. The total absorbed/scattered power [39] or force [5], [40] was obtained by numerically evaluating a surface integral over the body or over a bounding surface.

An alternative BEM approach to the computation of absorbed power was suggested by Ref. 41, which noted that the power absorbed by a compact body may be obtained directly from the surface currents, obviating the intermediate step of computing scattered fields. (This observation seems to have been mentioned as something of a passing curiosity in Ref. 41; although the authors note that the absorption may be computed directly from the surface currents, computational details are omitted, and thereafter the authors revert to the usual practice of obtaining absorption and other quantities via the intermediate device of computing scattered fields.)

Here we extend the observation of Ref. 41 by noting that powers, forces, and torques (PFTs) may be computed directly—in multiple ways—from the surface currents that are the primary output of the BEM solver, yielding PFT formulas of the form (1). We derive and compare these formulas in Section II, then illustrate their efficacy with a number of computational examples in Section III. All PFT formulas discussed in this paper are implemented in SCUFF-EM [1], a free, open-source BEM implementation.

II. PFTs FROM SURFACE-CURRENT BILINEARS

There are at least three distinct ways to write PFTs as surface-current bilinears of the form (1). In this section we discuss these and compare them qualitatively, saving quantitative comparisons for the following section.

Preliminaries; six-vector notation. Before beginning we state our context and introduce a shorthand notation that will streamline later discussions. We consider compact homogeneous bodies illuminated by known incident fields, working in the frequency domain with all fields and currents understood to have time dependence $\propto e^{-i\omega t}$. SIE formulations for dielectric bodies solve for electric and magnetic surface currents, obtained from tangential fields at body surfaces according to[1]

$$\mathbf{K}(\mathbf{x}) \equiv \hat{\mathbf{n}}(\mathbf{x}) \times \mathbf{H}(\mathbf{x}), \qquad \mathbf{N}(\mathbf{x}) \equiv -\hat{\mathbf{n}}(\mathbf{x}) \times \mathbf{E}(\mathbf{x}). \quad (3)$$

Here $\mathbf{x}$ lies on a body surface and $\hat{\mathbf{n}}(\mathbf{x})$ is the outward-pointing surface normal. In what follows it will be convenient to adopt a 6-vector notation for fields, currents, and dyadic Green's functions (DGFs):

$$\boldsymbol{\mathcal{F}} \equiv \begin{pmatrix} \mathbf{E} \\ \mathbf{H} \end{pmatrix}, \qquad \boldsymbol{\mathcal{C}} \equiv \begin{pmatrix} \mathbf{K} \\ \mathbf{N} \end{pmatrix}, \qquad \boldsymbol{\mathcal{G}} \equiv \begin{pmatrix} \boldsymbol{\Gamma}^{\mathrm{EE}} & \boldsymbol{\Gamma}^{\mathrm{EM}} \\ \boldsymbol{\Gamma}^{\mathrm{ME}} & \boldsymbol{\Gamma}^{\mathrm{MM}} \end{pmatrix} \quad (4)$$

with $\boldsymbol{\Gamma}^{\mathrm{AB}}$ the usual 3×3 DGF giving the A-type field due to a B-type current. In this language, equation (3) relating surface currents to surface fields reads

$$\boldsymbol{\mathcal{C}} = \boldsymbol{\mathcal{N}}^{\mathrm{P}} \boldsymbol{\mathcal{F}}, \qquad \boldsymbol{\mathcal{N}}^{\mathrm{P}}(\hat{\mathbf{n}}) \equiv \begin{pmatrix} 0 & \hat{\mathbf{n}}\times \\ -\hat{\mathbf{n}}\times & 0 \end{pmatrix} \quad (5)$$

(The significance of the "P" superscript on the 6×6 matrix $\boldsymbol{\mathcal{N}}^{\mathrm{P}}$ will become clear shortly.) We can also write a reciprocal relation, giving surface fields from surface currents, by noting from (3) that tangential fields are cross products of surface currents with $\pm\hat{\mathbf{n}}$, while normal fields are related to surface charge densities according to $\{\mathbf{E},\mathbf{H}\}\cdot\hat{\mathbf{n}} = \{\frac{\sigma_{\mathbf{K}}}{\epsilon}, \frac{\sigma_{\mathbf{N}}}{\mu}\}$ with $\sigma_{\mathbf{K},\mathbf{N}} = \frac{1}{i\omega}\nabla\cdot\{\mathbf{K},\mathbf{N}\}$. The inverse of (5) thus reads

$$\boldsymbol{\mathcal{F}} = \boldsymbol{\mathcal{M}}\boldsymbol{\mathcal{C}}, \qquad \boldsymbol{\mathcal{M}}\big(\hat{\mathbf{n}}\big) \equiv \begin{pmatrix} \frac{1}{i\omega\epsilon}\hat{\mathbf{n}}\,\nabla\cdot & \hat{\mathbf{n}}\times \\ -\hat{\mathbf{n}}\times & \frac{1}{i\omega\mu}\hat{\mathbf{n}}\,\nabla\cdot \end{pmatrix}. \quad (6)$$

In equation (6) we may use the values of ϵ, μ for either the exterior or interior medium; in either case we then obtain the limiting values of the surface fields as the surface is approached from that medium.

Equation (6) only applies to the fields on an object surface; off the surface, fields are related to currents by convolutions, which assume different forms depending on whether the evaluation point lies inside or outside an object $\mathcal{O}$:

$$\boldsymbol{\mathcal{F}}(\mathbf{x}) = \begin{cases} +\boldsymbol{\mathcal{G}}^{\mathrm{out}}(\mathbf{x},\mathbf{x}') \star \boldsymbol{\mathcal{C}}(\mathbf{x}') + \boldsymbol{\mathcal{F}}^{\mathrm{out}}_{\mathrm{sources}}(\mathbf{x}), & \mathbf{x} \notin \mathcal{O} \\ -\boldsymbol{\mathcal{G}}^{\mathrm{in}}(\mathbf{x},\mathbf{x}') \star \boldsymbol{\mathcal{C}}(\mathbf{x}') + \boldsymbol{\mathcal{F}}^{\mathrm{in}}_{\mathrm{sources}}(\mathbf{x}), & \mathbf{x} \in \mathcal{O} \end{cases}. \quad (7)$$

Here $\boldsymbol{\mathcal{G}}^{\mathrm{out,in}}$ are the DGFs for the homogeneous media outside and inside the body, $\star$ denotes convolution, and $\boldsymbol{\mathcal{F}}^{\mathrm{out,in}}_{\mathrm{sources}}$ are the fields of any sources lying outside and inside the body.

SIE formulations write integral equations relating surface currents to incident fields; for example, in the PMCHWT formulation [42] we have

$$\Big[\boldsymbol{\mathcal{G}}^{\mathrm{out}} + \boldsymbol{\mathcal{G}}^{\mathrm{in}}\Big]_{\parallel} \star \boldsymbol{\mathcal{C}} = -\boldsymbol{\mathcal{F}}^{\mathrm{inc}}_{\parallel} \quad (8)$$

[1]We use the symbols $\mathbf{K}$ and $\mathbf{N}$ for two-dimensional surface current densities, in contradistinction to the symbols $\mathbf{J}$ and $\mathbf{M}$ commonly used for three-dimensional volume current densities.

This article has been accepted for publication in a future issue of this journal, but has not been fully edited. Content may change prior to final publication. Citation information: DOI 10.1109/TAP.2015.2438393, IEEE Transactions on Antennas and Propagation

where $\|$ selects surface-tangential vector components. Numerical solvers approximate currents as finite expansions in a discrete set of $N_{\rm BF}$ basis functions,

$$\boldsymbol{\mathcal{C}}(\mathbf{x}) \approx \sum c_\alpha \boldsymbol{\mathcal{B}}_\alpha(\mathbf{x}), \tag{9}$$

where the six-vector basis set $\{\boldsymbol{\mathcal{B}}_\alpha\}$ typically contains separate three-vector functions for electric and magnetic currents, i.e. $\boldsymbol{\mathcal{B}} = \binom{\mathbf{b}}{0}$ or $\boldsymbol{\mathcal{B}} = \binom{0}{\mathbf{b}}$ where $\mathbf{b}$ is e.g. an RWG function [43]. The fields at a point $\mathbf{x}$ are related to the c_α coefficients by the discretized version of (7),

$$\boldsymbol{\mathcal{F}}(\mathbf{x}) = \begin{cases} \sum_\alpha c_\alpha \boldsymbol{\mathcal{F}}^{\rm out}_\alpha(\mathbf{x}) + \boldsymbol{\mathcal{F}}^{\rm out}_{\rm sources}(\mathbf{x}), & \mathbf{x} \notin \mathcal{O} \\ -\sum_\alpha c_\alpha \boldsymbol{\mathcal{F}}^{\rm in}_\alpha(\mathbf{x}) + \boldsymbol{\mathcal{F}}^{\rm in}_{\rm sources}(\mathbf{x}) & \mathbf{x} \in \mathcal{O} \end{cases} \tag{10}$$

where $\boldsymbol{\mathcal{F}}^{\rm in,out}_\alpha = \boldsymbol{\mathcal{G}}^{\rm in,out} \star \boldsymbol{\mathcal{B}}_\alpha$ is the six-vector of fields due to a single unit-strength basis function. Upon discretization, the integral equation (8) becomes an $N_{\rm BF} \times N_{\rm BF}$ linear system for the $\{c_\alpha\}$ coefficients:

$$\Big(\mathbf{M}^{\rm out} + \mathbf{M}^{\rm in}\Big)\mathbf{c} = -\mathbf{f}^{\rm inc} \tag{11}$$

where $\mathbf{f}^{\rm inc}$ describes the projections of the incident fields onto the basis functions.

A. Displaced surface-integral PFT

A conceptually straightforward approach to computing PFTs for an object $\mathcal{O}$ is simply to integrate the Poynting vector (PV) $\mathbf{P}$ or Maxwell stress tensor (MST) $\mathbf{T}$ over a bounding surface $\mathcal{S}$ surrounding the object but displaced from the object surface. At a point on $\mathcal{S}$ at which the outward-pointing surface normal is $\hat{\mathbf{n}}$, the fluxes of energy and $\hat{\mathbf{u}}$-directed linear momentum are

$$\mathbf{P}\cdot\hat{\mathbf{n}} = \Big(\mathbf{E}^* \times \mathbf{H}\Big)\cdot\hat{\mathbf{n}} \tag{12a}$$

$$\hat{\mathbf{u}}\cdot\mathbf{T}\cdot\hat{\mathbf{n}} = \hat{u}_i\left\{\epsilon E_i^* E_j + \mu H_i^* H_j - \frac{\delta_{ij}}{2}\Big[\epsilon|\mathbf{E}|^2 + \mu|\mathbf{H}|^2\Big]\right\}\hat{n}_j. \tag{12b}$$

Here ϵ, μ are the absolute material properties of the medium outside $\mathcal{O}$—which we assume to be lossless, as the definition of the stress tensor in lossy media is problematic [44]—and summation over repeated indices is implied. [The flux of $\hat{\mathbf{u}}$-directed *angular* momentum about an origin $\mathbf{x}_0$, useful for torque computations, follows from (12b) with the replacement $\mathbf{T} \to (\mathbf{x}-\mathbf{x}_0)\times\mathbf{T}$; in general, all of our force formulas have immediate torque analogues, which we will not write explicitly.] The time-average power absorbed by, and the $\hat{\mathbf{u}}$-directed force on, all bodies contained in $\mathcal{S}$ are

$$\begin{aligned} P^{\rm abs} &= -\frac{1}{2}{\rm Re}\oint_{\mathcal{S}} \mathbf{P}(\mathbf{x})\cdot\hat{\mathbf{n}}\,dA, \\ &= +\frac{1}{4}\oint_{\mathcal{S}}\Big\{\boldsymbol{\mathcal{F}}^\dagger(\mathbf{x})\boldsymbol{\mathcal{N}}^{\rm P}(\hat{\mathbf{n}})\boldsymbol{\mathcal{F}}(\mathbf{x})\Big\}\,dA \end{aligned} \tag{13a}$$

$$\begin{aligned} \mathbf{F}\cdot\hat{\mathbf{u}} &= \frac{1}{2}{\rm Re}\oint_{\mathcal{S}} \hat{\mathbf{u}}\cdot\mathbf{T}(\mathbf{x})\cdot\hat{\mathbf{n}}\,dA \\ &= \frac{1}{4}\oint_{\mathcal{S}}\Big\{\boldsymbol{\mathcal{F}}^\dagger(\mathbf{x})\boldsymbol{\mathcal{N}}^{\rm F}(\hat{\mathbf{u}},\hat{\mathbf{n}})\boldsymbol{\mathcal{F}}(\mathbf{x})\,dA\Big\} \end{aligned} \tag{13b}$$

where we have expressed the PV and MST (12) in the six-vector notation introduced above; the "power" matrix $\boldsymbol{\mathcal{N}}^{\rm P}$ is the same matrix that appears in (5), while the "force" matrix $\boldsymbol{\mathcal{N}}^{\rm F}$ is

$$\boldsymbol{\mathcal{N}}^{\rm F}(\hat{\mathbf{u}},\hat{\mathbf{n}}) \equiv \begin{pmatrix} \epsilon\mathbf{N}^{\rm F}(\hat{\mathbf{u}},\hat{\mathbf{n}}) & 0 \\ 0 & \mu\mathbf{N}^{\rm F}(\hat{\mathbf{u}},\hat{\mathbf{n}}) \end{pmatrix}, \tag{14}$$

$$\mathbf{N}^{\rm F}(\hat{\mathbf{u}},\hat{\mathbf{n}}) = \hat{\mathbf{u}}\hat{\mathbf{n}}^\dagger + \hat{\mathbf{n}}\hat{\mathbf{u}}^\dagger - (\hat{\mathbf{u}}\cdot\hat{\mathbf{n}})\mathbf{1} \tag{15}$$

where $\dagger$ denotes vector transposition and $\mathbf{1}$ is the 3×3 unit matrix. [The 6×6 "torque" matrix $\boldsymbol{\mathcal{N}}^{\rm T}$ has the same block structure as (14) with $\mathbf{x}$-dependent 3×3 subblocks $\mathbf{N}^{\rm T}$.] If $\mathbf{x}$ lies in a region in which there are no incident-field sources, then the total fields at $\mathbf{x}$ are given by summing surface-current contributions [equation (10) with no sources], and the $\hat{\mathbf{n}}$-directed power flux at $\mathbf{x}$ reads

$$\begin{aligned} \frac{1}{2}{\rm Re}\ \mathbf{P}(\mathbf{x})\cdot\mathbf{n}(\mathbf{x}) &= \sum_{\alpha\beta} c_\alpha^* \underbrace{\Big[-\boldsymbol{\mathcal{F}}^\dagger_\alpha(\mathbf{x})\boldsymbol{\mathcal{N}}^{\rm P}(\hat{\mathbf{n}})\boldsymbol{\mathcal{F}}_\beta(\mathbf{x})\Big]}_{Q^{\rm PFLUX}_{\mathbf{x};\alpha\beta}} c_\beta \\ &= \mathbf{c}^\dagger\mathbf{Q}^{\rm PFLUX}_{\mathbf{x}}\mathbf{c}. \end{aligned} \tag{16}$$

Integrating over $\mathcal{S}$, the total absorbed power reads

$$\begin{aligned} P^{\rm abs} &= \sum_{\alpha\beta} c_\alpha^* \left[\oint_{\mathcal{S}} \boldsymbol{\mathcal{F}}^\dagger_\alpha(\mathbf{x})\boldsymbol{\mathcal{N}}^{\rm P}(\hat{\mathbf{n}})\boldsymbol{\mathcal{F}}_\beta(\mathbf{x})\,d\mathbf{x}\right] c_\beta \\ &\approx \sum_{\alpha\beta} c_\alpha^* \underbrace{\sum_{n=1}^{N_{\rm C}}\Big[w_n \boldsymbol{\mathcal{F}}^\dagger_\alpha(\mathbf{x}_n)\boldsymbol{\mathcal{N}}^{\rm P}(\hat{\mathbf{n}})\boldsymbol{\mathcal{F}}_\beta(\mathbf{x}_n)\Big]}_{Q^{\rm PABS}_{{\rm DSI};\alpha\beta}} c_\beta \\ &= \mathbf{c}^\dagger\mathbf{Q}^{\rm PABS}_{\rm DSI}\mathbf{c}. \end{aligned} \tag{17}$$

where we have used an $N_{\rm C}$-point cubature rule with weights and points $\{w_n, \mathbf{x}_n\}$ to integrate over $\mathcal{S}$. Equations (16) and (17) express the local Poynting flux and the total absorbed power as surface-current bilinears of the form (1), with equations for the force and torque following by replacing $\boldsymbol{\mathcal{N}}^{\rm P} \to \boldsymbol{\mathcal{N}}^{\rm F,T}$; we refer to these as the "displaced surface integral PFT" (DSIPFT) expressions. If there are incident-field sources in the region, their contributions must be added to (16) and (17).

B. Overlap PFT

We obtain a considerable simplification by allowing the bounding surface $\mathcal{S}$ in equation (13) to coincide with the object surface $\partial\mathcal{O}$. In this case, the PV and MST in the integrand involve only the fields at the object surface, and the convolution step taking fields to currents [equation (7)] may be bypassed in favor of equation (6) yielding surface fields *directly* from surface currents. Taking $\mathcal{S} \to \partial\mathcal{O}$ and using (6) in (13) yields power and force expressions involving only surface currents:

$$P^{\rm abs} = \frac{1}{4}\oint_{\partial\mathcal{O}}\Big[\boldsymbol{\mathcal{C}}^\dagger(\mathbf{x})\,\boldsymbol{\mathcal{N}}^{\rm P}(\hat{\mathbf{n}})\,\boldsymbol{\mathcal{C}}(\mathbf{x})\Big]\,dA \tag{18a}$$

$$\mathbf{F}\cdot\hat{\mathbf{u}} = \frac{1}{4}\oint_{\partial\mathcal{O}}\Big\{\boldsymbol{\mathcal{C}}^\dagger(\mathbf{x})\Big[\boldsymbol{\mathcal{M}}^\dagger\boldsymbol{\mathcal{N}}^{\rm F}(\hat{\mathbf{u}},\hat{\mathbf{n}})\boldsymbol{\mathcal{M}}\Big]\boldsymbol{\mathcal{C}}(\mathbf{x})\Big\}dA. \tag{18b}$$

This article has been accepted for publication in a future issue of this journal, but has not been fully edited. Content may change prior to final publication. Citation information: DOI 10.1109/TAP.2015.2438393, IEEE Transactions on Antennas and Propagation

In three-vector notation, these expressions read

$$P^{\text{abs}} = \frac{1}{2}\text{Re}\ \oint_{\partial\mathcal{O}} \mathbf{K}^*(\mathbf{x}) \cdot \Big[\hat{\mathbf{n}} \times \hat{\mathbf{N}}(\mathbf{x})\Big]\, dA$$

$$\mathbf{F}\cdot\hat{\mathbf{u}} = \frac{1}{2}\text{Re}\ \oint_{\partial\mathcal{O}} \Big\{\sigma^*_{\mathbf{K}}\Big[\hat{\mathbf{u}}\cdot(\hat{\mathbf{n}}\times\mathbf{N})\Big] - \sigma^*_{\mathbf{N}}\Big[\hat{\mathbf{u}}\cdot(\hat{\mathbf{n}}\times\mathbf{K})\Big] - \frac{\hat{\mathbf{u}}\cdot\hat{\mathbf{n}}}{2}\left[\mu\Big(|\mathbf{K}|^2 - \frac{|\nabla\cdot\mathbf{K}|^2}{k^2}\Big) + \epsilon\Big(|\mathbf{N}|^2 - \frac{|\nabla\cdot\mathbf{N}|^2}{k^2}\Big)\right]\Big\}\, dA$$

where $\sigma_{\mathbf{K},\mathbf{N}} = \frac{1}{i\omega}\nabla\cdot\{\mathbf{K},\mathbf{N}\}$ and ϵ,μ are again the *exterior* material properties. Inserting the basis-function expansion (9) into formula (18a), we obtain a surface-current bilinear expression of the form (1) for the absorbed power:

$$P^{\text{abs}} = \sum_{\alpha\beta} c^*_\alpha \underbrace{\left[\frac{1}{4}\oint_{\partial\mathcal{O}} \boldsymbol{\mathcal{B}}^\dagger_\alpha \boldsymbol{\mathcal{N}}^{\text{P}} \boldsymbol{\mathcal{B}}_\beta\, dA\right]}_{Q^{\text{PABS}}_{\text{Overlap};\alpha\beta}} c_\beta = \mathbf{c}^\dagger \mathbf{Q}^{\text{PABS}}_{\text{Overlap}} \mathbf{c} \tag{20}$$

again with similar formulas for the force and torque following from the replacement $\boldsymbol{\mathcal{N}}^{\text{P}} \to \boldsymbol{\mathcal{N}}^{\text{T,F}}$. We refer to equation (20) and its force and torque analogues as "overlap PFT" (OPFT) formulas.

An immediate advantage of the OPFT approach is that the elements of the $\mathbf{Q}_{\text{Overlap}}$ matrices involve only local operators (no convolutions) sandwiched between basis functions ("overlap integrals" or "Gram matrix elements"), and hence these matrices are typically *sparse*. (This is the origin of the term "overlap PFT.") For example, in three-vector notation the elements of $\mathbf{Q}^{\text{PABS}}_{\text{Overlap}}$ read

$$Q^{\text{PABS}}_{\text{Overlap};\alpha\beta} = \pm\frac{1}{4}\int_{\sup \mathbf{b}_\alpha} d\mathbf{x} \int_{\sup \mathbf{b}_\beta} d\mathbf{x}' \Big[\mathbf{b}_\alpha(\mathbf{x}) \times \mathbf{b}_\beta(\mathbf{x}')\Big]\cdot\hat{\mathbf{n}} \equiv \frac{1}{4}\big\langle \hat{\mathbf{n}}\cdot\big(\mathbf{b}_\alpha\times\mathbf{b}_\beta\big)\big\rangle \tag{21}$$

where $\{\mathbf{b}_\alpha,\mathbf{b}_\beta\}$ are three-vector (i.e. RWG) basis functions and $\langle,\rangle$ denotes an integral over basis-function supports. [Elements of the $\mathbf{Q}_{\text{Overlap}}$ matrices for the i component of the force involve additional overlap integrals of the form

$$\Big\langle \big[\nabla\cdot\mathbf{b}_\alpha\big](\hat{\mathbf{n}}\times\mathbf{b}_\beta)_i\Big\rangle,\ \big\langle \hat{n}_i\big(\mathbf{b}_\alpha\cdot\mathbf{b}_\beta\big)\big\rangle,\ \big\langle \hat{n}_i\big(\nabla\cdot\mathbf{b}_\alpha\big)\big(\nabla\cdot\mathbf{b}_\beta\big)\big\rangle \tag{22}$$

and the torque case is similar.] If the basis functions are localized, then the overlap integrals vanish for all but a small number of pairs of neighboring basis functions. For example, RWG functions have nonzero overlaps with at most 5 other RWG functions (twice that number considering electric and magnetic currents), so for these functions the matrix in (20) has at most 10 nonzero entries per row. For the particular case of RWG functions, all overlap matrix elements are simple polynomial integrals that may be easily evaluated in closed analytical form.

An additional advantage of the OPFT approach is that, in contrast to e.g. the DSIPFT expression (17), equation (20) does *not* require modification to account for incident-field sources in any region; indeed, because the surface currents are always the tangential components of the *total* fields, they already reflect the contributions of any such sources that may be present.

C. Equivalence-principle PFT

The overlap PFT formulas (18) follow from the DSIPFT formulas (13) by replacing both field six-vectors $\boldsymbol{\mathcal{F}}$ in (13) with current six-vectors $\boldsymbol{\mathcal{C}}$. If we instead replace only *one* factor of $\boldsymbol{\mathcal{F}}$ with $\boldsymbol{\mathcal{C}}$, we obtain yet a third set of formulas, whose physical significance we may understand by appealing to the equivalence-principle interpretation of the SIE formalism [13], [45]; in this picture, a solid dielectric body $\mathcal{O}$ with surface $\partial\mathcal{O}$ is replaced by an *empty* volume $\mathcal{O}$ and equivalent electric and magnetic currents $\{\mathbf{K},\mathbf{N}\}$ flowing on $\partial\mathcal{O}$. The PFT on $\mathcal{O}$ may then be computed as the work done on, and the force and torque exerted on, the surface currents by the external fields. In particular, the power absorbed by $\mathcal{O}$ is just the usual Joule heating of the surface currents, while the force on $\mathcal{O}$ follows from the Lorentz force on the currents:

$$P^{\text{abs}} = \frac{1}{4}\text{Re}\ \oint_{\partial\mathcal{O}} \{\mathbf{K}^*\cdot\mathbf{E} + \mathbf{N}^*\cdot\mathbf{H}\}\, dA \tag{23a}$$

$$\mathbf{F} = \frac{1}{4}\text{Re}\ \oint_{\partial\mathcal{O}} \Big\{\sigma^*_{\mathbf{K}}\mathbf{E} + \mu\Big(\mathbf{K}^*\times\mathbf{H}\Big) + \sigma^*_{\mathbf{N}}\mathbf{H} - \epsilon\Big(\mathbf{N}^*\times\mathbf{E}\Big)\Big\}\, dA \tag{23b}$$

{To understand equations (23), recall that the time-average absorbed power and force on a *volume* electric current distribution $\mathbf{J}$ would be given by the usual Joule heating $P^{\text{abs}} = \frac{1}{2}\text{Re}\ \int(\mathbf{J}^*\cdot\mathbf{E})\, dV$ and the usual Lorentz force $\mathbf{F} = \frac{1}{2}\text{Re}\ \int(\rho^*\mathbf{E} + \mu\,\mathbf{J}^*\times\mathbf{H})\, dV$; equation (23) simply modifies these relations by adding magnetic-current terms, replacing volume with surface integrations, and including an extra factor of $\frac{1}{2}$ to account for a well-known subtlety involving the fields at body surfaces [45].} In six-vector language, equations (23) read

$$P^{\text{abs}} = \frac{1}{4}\text{Re}\ \oint_{\partial\mathcal{O}} \boldsymbol{\mathcal{C}}^\dagger\boldsymbol{\mathcal{F}}\, dA \tag{24a}$$

$$\mathbf{F}\cdot\hat{\mathbf{u}} = -\frac{1}{4}\text{Re}\ \oint_{\partial\mathcal{O}} \boldsymbol{\mathcal{C}}^\dagger\boldsymbol{\mathcal{M}}^\dagger(\hat{\mathbf{u}}) \begin{pmatrix} \epsilon & 0 \\ 0 & \mu \end{pmatrix} \boldsymbol{\mathcal{F}}\, dA \tag{24b}$$

We refer to equations (24) as the "equivalence-principle PFT" (EPPFT) formulas.

Because these formulas involve the fields at the surface, in principle we have the choice of using either the exterior or interior expansion for $\boldsymbol{\mathcal{F}}$ (equation 10). For the *power*, which involves only tangential field components, the two expansions yield equivalent results (because tangential field components are continuous across surfaces) and the choice is dictated by convenience: we use whichever of the two expansions does not contain incident-field terms. In particular, for typical cases involving incident-field sources outside the body, we choose the interior expansion. On the other hand, the force and torque expressions involve normal field components; since the interior and exterior branches of (10) yield inequivalent results for these quantities (and we require the exterior fields), here we must use the exterior expansion.

Of course, the apparent novelty of the EPPFT expressions (24) versus the DSIPFT expressions (13) or the OPFT expressions (18) is only superficial; if, in (24), we use (6) to replace currents with fields, then after some algebra we recover equations (13) for the case $\mathcal{S} = \partial\mathcal{O}$, while instead using (5)

This article has been accepted for publication in a future issue of this journal, but has not been fully edited. Content may change prior to final publication. Citation information: DOI 10.1109/TAP.2015.2438393, IEEE Transactions on Antennas and Propagation

to replace fields with currents leads us back to the overlap formulas (18). However, the form of (24) as written suggests a *computational* procedure with distinct ramifications: If we evaluate the *currents* in (24) as in the OPFT method [the basis-function expansion (9)], but evaluate the *fields* as in the SIPFT method [the convolution (10)], we obtain a hybrid method with features intermediate between those of the other approaches. Inserting (9) and (10) in (24a), we find

$$P^{\text{abs}} = \sum_{\alpha\beta} c_\alpha^* \underbrace{\left[\frac{1}{4}\oint_{\partial\mathcal{O}} \boldsymbol{\mathcal{B}}_\alpha^\dagger \boldsymbol{\mathcal{G}} \boldsymbol{\mathcal{B}}_\beta \, dA\right]}_{Q_{\text{EP}}^{\text{PABS}};\alpha\beta} c_\beta$$
$$= \mathbf{c}^\dagger \mathbf{Q}_{\text{EP}}^{\text{PABS}} \mathbf{c} \tag{25}$$

again with similar expressions for the force and torque. The elements of the $\mathbf{Q}_{\text{EP}}$ matrices involve the projections onto basis functions of the fields of other basis functions; for example, the elements of the power matrix $\mathbf{Q}_{\text{EP}}^{\text{PABS}}$ involve the quantities

$$\Big\langle \mathbf{b}_\alpha \cdot \mathbf{E}_\beta \Big\rangle \quad \text{and} \quad \Big\langle \mathbf{b}_\alpha \cdot \mathbf{H}_\beta \Big\rangle \tag{26}$$

where $\mathbf{b}_\alpha$ is a three-vector (i.e. RWG) basis function and $\{\mathbf{E}, \mathbf{H}\}_\beta$ are the fields due to basis function $\mathbf{b}_\beta$ populated with unit strength. [For the $\mathbf{u}$-directed force we additionally require

$$\Big\langle (\nabla \cdot \mathbf{b}_\alpha)(\hat{\mathbf{u}} \cdot \mathbf{E}_\beta) \Big\rangle, \qquad \Big\langle \hat{\mathbf{u}} \cdot (\mathbf{b}_\alpha \times \mathbf{E}_\beta) \Big\rangle \tag{27}$$

and their analogs with $\mathbf{E}_\beta \to \mathbf{H}_\beta$; the torque case is similar.] The quantities in equations (26) and (27) involve four-dimensional integrals which, in contrast to overlap integrals like (21), generally cannot be evaluated in closed form, and which moreover involve integrand singularities if $\mathbf{b}_\alpha, \mathbf{b}_\beta$ have nonzero overlap. Although the BEM literature abounds with techniques for computing singular integrals of this form [46]–[48], the need to implement such specialized techniques for computing matrix elements makes the EPPFT the least computationally convenient of the approaches we consider.

An exception to this statement applies if we need only to compute the power, not the force or torque. In this case, the quantities we need for the EP computation—equation (26)—happen to be precisely the quantities needed to compute matrix elements of the discretized BEM matrices in the PMCHWT formulation, equation (11). Thus, for a problem involving incident-field sources lying outside an object $\mathcal{O}$, the power absorbed by $\mathcal{O}$ may be computed in the form

$$\mathbf{P}^{\text{abs}} = -\frac{1}{4}\mathbf{c}^\dagger \mathbf{M}^{\text{in}} \mathbf{c} \tag{28}$$

where $\mathbf{M}^{\text{in}}$ is the "interior" contribution to the BEM matrix in (11), describing the interactions of surface currents on $\mathcal{O}$ interacting via the DGF for the material medium interior to $\mathcal{O}$. Since this matrix must be computed to solve the system in the first place, equation (28) amounts to an easy post-processing computation of absorbed power.

D. Comparison of PFT formulas

The DSIPFT expression (17), the OPFT expression (20), and the EPPFT expression (25) represent three distinct ways of writing matrices $\mathbf{Q}$ that, when sandwiched between surface-current vectors $\mathbf{c}$ as in (1), yield the time-average absorbed power on a body $\mathcal{O}$ (similarly, we have three distinct ways of writing $\mathbf{Q}$ matrices for the force and torque). With exact representations of currents and fields and exact surface integrations, all three formulas must of course predict identical PFTs. In actual calculations involving finite basis sets and finite numerical cubature, their predictions will differ, as will their computational cost. To characterize these distinctions it is useful to compare the expressions for the α, β matrix element of e.g. the $\mathbf{Q}^{\text{PABS}}$ matrix obtained in each formalism:

$$Q_{\alpha\beta}^{\text{PABS}} = \begin{cases} \displaystyle\sum_{n=1}^{N_{\text{C}}} \frac{w_n}{4} \oint_{\partial\mathcal{O}} \oint_{\partial\mathcal{O}} \boldsymbol{\mathcal{B}}_\alpha^\dagger \boldsymbol{\mathcal{G}}^\dagger \boldsymbol{\mathcal{N}}^{\text{P}} \boldsymbol{\mathcal{G}} \boldsymbol{\mathcal{B}}_\beta \, dA \, dA' & \text{DSIPFT} \\ \displaystyle\frac{1}{4}\oint_{\partial\mathcal{O}} \boldsymbol{\mathcal{B}}_\alpha^\dagger \boldsymbol{\mathcal{G}} \boldsymbol{\mathcal{B}}_\beta \, dA, & \text{EPPFT} \\ \displaystyle\frac{1}{4}\oint_{\partial\mathcal{O}} \boldsymbol{\mathcal{B}}_\alpha^\dagger \boldsymbol{\mathcal{N}}^{\text{P}} \boldsymbol{\mathcal{B}}_\beta \, dA, & \text{OPFT.} \end{cases} \tag{29}$$

[For the DSIPFT case we have here explicitly written out the convolutions implicit in the quantities $\boldsymbol{\mathcal{F}}_{\alpha,\beta}$ in (17).] The key distinction between these formulas is the number of appearances of $\boldsymbol{\mathcal{G}}$, each of which signifies a convolution step: in the {O, EP, DSI} expressions, $\boldsymbol{\mathcal{G}}$ appears {0, 1, 2} times. These differences determine the relative cost and accuracy of the various approaches.

Cost. The overlap PFT computation involves no convolutions; instead, as noted above, the matrix elements are simple overlap integrals between basis functions, which may typically be evaluated in closed analytical form (in particular, this is possible for RWG functions). Moreover, for localized basis functions the OPFT matrices are *sparse*, ensuring that (1) is an $O(N_{\text{BF}})$ operation. Thus the OPFT approach is by far the fastest of the PFT approaches.

The EPPFT computation involves one convolution, and the matrix elements in this case are of the form (26-27), describing the $\boldsymbol{\mathcal{G}}-$interactions of the basis functions. These are four-dimensional integrals over basis functions—with integrand singularities present if the functions overlap—whose evaluation adds significant computational cost and inconvenience for force and torque calculations. (However, as noted above, for *power* computations the same integrals are already computed as part of the BEM system solution, so this case requires no further computation.) In contrast to the OPFT case, the $\mathbf{Q}_{\text{EP}}$ matrices are dense, so the cost of evaluating (1) is $O(N_{\text{BF}}^2)$ in this case.

In the DSIPFT case each matrix element involves *two* convolutions plus a sum over N_{C} cubature points, so here the naïve cost of evaluating (1) is $O(N_{\text{C}} N_{\text{BF}}^2)$.

Of course, this discussion assumes that we compute PFTs using the vector-matrix-vector product formulas (1), with each element of the $\mathbf{Q}$ matrix computed explicitly. For EPPFT and DSIPFT calculations in classical, deterministic problems—the context of equation (1)—it will typically be faster to do the computation without forming this matrix. For example, to evaluate the DSIPFT or EPPFT integrals (13) or (24) using an N_{C}-point cubature rule for $\oint_{\mathcal{S}}$ or $\oint_{\partial\mathcal{O}}$, we would first do

This article has been accepted for publication in a future issue of this journal, but has not been fully edited. Content may change prior to final publication. Citation information: DOI 10.1109/TAP.2015.2438393, IEEE Transactions on Antennas and Propagation

a single $O(N_{\rm C}N_{\rm BF})$ step to compute and store the fields at all cubature points, then a second $O(N_{\rm C})$ step to evaluate the integrand at each cubature point. However, for applications to fluctuation-induced phenomena [the context of equation (2)], such an approach is not possible; here we must separately compute the contribution of each individual pair of basis functions to evaluate the matrix product trace in (2), and in this case both DSIPFT and EPPFT are $O(N_{\rm BF}^2)$ operations, while OPFT remains $O(N_{\rm BF})$.

Accuracy. The number of occurrences of $\boldsymbol{\mathcal{G}}$ also affects the accuracy of the formulas. Indeed, each time we eliminate a $\boldsymbol{\mathcal{G}}$ factor in equation (29) (going from 2 to 1 to 0 factors as we progress from DSIPFT to EPPFT to OPFT) we are replacing one current-to-field convolution (10) with one instance of the direct current-to-field relationship (6), with each such replacement contributing some loss of accuracy. Indeed, the relations between surface currents and total tangential fields, equations (5) and (6), are only approximately satisfied in a finite solver, and in particular the surface fields as computed from the direct relation (5) are less accurate than those computed from the convolution (10). [This is true even though the procedures of (5) and (10) use the same surface-current inputs, which in a finite solver are themselves only approximations of the exact surface currents; the error present in these approximations is compounded by using the additional approximation (5) instead of the convolution (10).] Thus in principle we might expect the accuracy hierarchy to be DSIPFT $>$ EPPFT $>$ OPFT.

This naïve expectation is complicated by other considerations. The DSIPFT case involves a numerical cubature over the bounding surface $\mathcal{S}$, while the EPPFT case involves a numerical cubature over the object surface $\partial\mathcal{O}$ [or, equivalently, numerical cubatures over basis-function supports of the form (26-27)], and these numerical integrations introduce additional errors. In contrast, the OPFT involves only overlap integrals of the form (21-22), which (for RWG and other simple basis functions) may be evaluated *exactly* in closed form, ensuring no additional error contribution. In practice this advantage seems to compensate the other sources of inaccuracy expected for OPFT calculations, which we typically find to be as accurate, if not more accurate, than calculations using the other approaches. Since the OPFT is also by far the fastest approach, in general it will thus be the optimal choice, although exceptions exist in particular cases as discussed in the following section.

E. Other power formulas

The power formulas considered thus far have been for the absorbed power; here we note some similar expressions for other physical quantities of interest.

Total power (extinction). The total (absorbed plus scattered) power extinguished by a body from an incident field may be computed as the work done on the surface currents by the incident fields. Replacing total fields with incident fields in (24a), we find

$$P^{\rm tot} = \frac{1}{2}{\rm Re}\oint \boldsymbol{\mathcal{C}}^\dagger \boldsymbol{\mathcal{F}}^{\rm inc}\, dA \tag{30}$$

$$= \frac{1}{2}\mathbf{c}^\dagger \mathbf{f}^{\rm inc} \tag{31}$$

$$= -\frac{1}{2}\mathbf{c}^\dagger \mathbf{M}\mathbf{c} \tag{32}$$

where $\mathbf{f}^{\rm inc}$, the projection of the incident fields onto the basis functions, is just the negative of the RHS vector in the discretized system (11); in equation (32) we have used equation (11) to write the total power as a surface-current bilinear of the form (1) involving the BEM system matrix $\mathbf{M} = \mathbf{M}^{\rm in} + \mathbf{M}^{\rm out}$. As both $\mathbf{c}$ and $\mathbf{f}^{\rm inc}$ are computed with the solution of (11), equation (31) represents an $O(N_{\rm BF})$ post-processing step with no further computation required. On the other hand, the form of equation (32) and the fact that the BEM matrix in the PMCHWT formulation is negative definite [11] ensure that the total power is always positive, as expected on physical grounds.

Scattered / radiated power. For a problem involving incident-field sources lying outside a body, the scattered power is the difference between the total and absorbed power. In the OPFT formalism, we may subtract (20) from (31) to yield

$$P^{\rm scat}_{\rm Overlap} = P^{\rm tot} - P^{\rm abs}_{\rm Overlap} = \mathbf{c}^\dagger\left[\frac{1}{2}\mathbf{f}^{\rm inc} - \mathbf{Q}^{\rm PABS}_{\rm Overlap}\mathbf{c}^\dagger\right] \tag{33}$$

again an $O(N_{\rm BF})$ operation since since $\mathbf{Q}^{\rm PABS}_{\rm Overlap}$ is sparse. Alternatively, in the EPPFT formalism, we have

$$P^{\rm scat}_{\rm EP} = P^{\rm tot} - P^{\rm abs}_{\rm EP} = \mathbf{c}^\dagger\left[\frac{1}{2}\mathbf{f}^{\rm inc} - \mathbf{Q}^{\rm PABS}_{\rm EP}\mathbf{c}\right] \tag{34}$$

$$= -\frac{1}{4}\mathbf{c}^\dagger \mathbf{M}^{\rm out}\mathbf{c} \tag{35}$$

where we used equations (11) and (28). Equation (35) for the scattered power is complementary to (28) for the absorbed power; since the matrix $\mathbf{M}^{\rm out}$ is already computed in the process of solving (11), equation (35) is an $O(N_{\rm BF}^2)$ post-processing step requiring no further computation.

If the incident-field sources lie *inside* the body, we may think of equation (35) as the equivalent of equation (28) with interior and exterior media reversed; this is then the power "absorbed" by the exterior medium from the incident-field sources, or in other words the power radiated into the exterior medium from the sources inside the body.

Scattering amplitude. The amplitude for scattering in the $\hat{\mathbf{k}}$ direction with a given polarization is obtained by projecting the surface currents onto the fields of a $\hat{\mathbf{k}}-$traveling plane wave of that polarization [49]:

$$F(\hat{\mathbf{k}}) = \frac{iZk}{4\pi}\oint \boldsymbol{\mathcal{C}}^\dagger \boldsymbol{\mathcal{F}}^{\rm PW}_{\hat{\mathbf{k}}}\, dA \tag{36}$$

$$= \frac{iZk}{4\pi}\mathbf{c}^\dagger \mathbf{f}^{\rm PW}_{\hat{\mathbf{k}}}. \tag{37}$$

where $\mathbf{f}^{\rm PW}_{\hat{\mathbf{k}}}$ is the RHS vector in (11) that would be computed if the incident field were a $\hat{\mathbf{k}}-$traveling plane wave.

Relation to the optical theorem. In a scattering problem in which the surface currents $\boldsymbol{\mathcal{C}}$ are induced by an incident field consisting of a $\hat{\mathbf{k}}$-traveling plane wave, equation (37) gives the

This article has been accepted for publication in a future issue of this journal, but has not been fully edited. Content may change prior to final publication. Citation information: DOI 10.1109/TAP.2015.2438393, IEEE Transactions on Antennas and Propagation

forward scattering amplitude. On the other hand, the vector inner product in (37) is just twice the extinction as computed by (31). Comparing (31) and (37) in this case, we find

$$P^{\rm tot} = \frac{2\pi}{kZ}{\rm Im}\ F(\hat{\mathbf{k}}).$$

This is the well-known optical theorem, relating the extinction to the imaginary part of the forward scattering amplitude [49].

III. Computational Examples

A. Energy and Momentum Transfer in Mie Scattering

We first validate and compare our formulas by using them to reproduce well-known results for a sphere irradiated by a plane wave (Mie scattering). Analytical formulas for the absorbed power, scattered power, and force (radiation pressure) in this case may be found in standard textbooks [12].

Figures 1 and 2 plot the efficiencies of scattering, absorption, and z-directed force on a spherical nanoparticle of radius $R = 1\,\mu$m, irradiated by a linearly-polarized z-traveling plane wave with electric field $\mathbf{E}^{\rm inc}(\mathbf{x},\mathbf{t}) = E_0\hat{\mathbf{x}}e^{i(kz-\omega t)}$. The nanoparticle is composed of gold, modeled as a lossy dielectric with frequency-dependent permittivity

$$\epsilon_{\rm gold} = \epsilon_0\left(1 - \frac{\omega_p^2}{\omega(\omega+i\gamma)}\right) \qquad (38)$$

with $\{\omega_p,\gamma\} = \{1.37\cdot 10^{16}, 5.32\cdot 10^{13}\}$ rad / sec. Dashed black lines indicate the results of Mie theory [12], while data points indicate results obtained from the methods proposed in this paper, using RWG basis functions for a sphere discretized into N=206 triangular panels (inset). (For the DSIPFT we take the bounding surface $\mathcal{S}$ to be a sphere of radius $10R$ and use a Lebedev [50] cubature rule with $N_{\rm C}$=302 points.) Absorption and scattering cross sections $\sigma^{\rm abs,scat}$ are obtained by dividing the total absorbed and scattered power by the incident power flux, $\sigma^{\rm abs,scat} = P^{\rm abs,scat}/I^{\rm inc}$, where $I^{\rm inc} = \frac{|E_0|^2}{2Z_0}$ for a plane wave in vacuum. The force cross section is obtained by dividing the total z-directed force on the particle by the incident momentum flux, $\sigma^{\rm force} = F_z/I_{\rm M}^{\rm inc}$ with $I_{\rm M}^{\rm inc} = \frac{|E_0|^2}{2Z_0c}$ for a plane wave in vacuum. Efficiencies $Q^{\rm abs,scat,force}$ are obtained from cross sections $\sigma^{\rm abs,scat,force}$ by dividing by the geometrical cross section presented by the particle, $Q = \sigma/(\pi R^2)$.

For power computations, the three methods we consider yield equivalent accuracy at most frequencies. The exceptions are **(a)** the low-frequency tail of the scattering efficiency, where OPFT becomes inaccurate, and **(b)** the high-frequency tail of the absorption efficiency, where both OPFT and DSIPFT become inaccurate. Errors in the former case arise because the low-frequency extinction is dominated by absorption, so the OPFT scattered-power expression (33) involves the subtraction of two nearly equal numbers and thus incurs numerical inaccuracies that are absent from the EPPFT expression (35). Errors in the latter case arise because at high frequencies the DSIPFT integrand oscillates over the bounding-sphere surface more rapidly than can be resolved by our fixed-order cubature scheme.

For force computations, at low frequencies both OPFT and EPPFT exhibit slight inaccuracies due to imperfect resolution

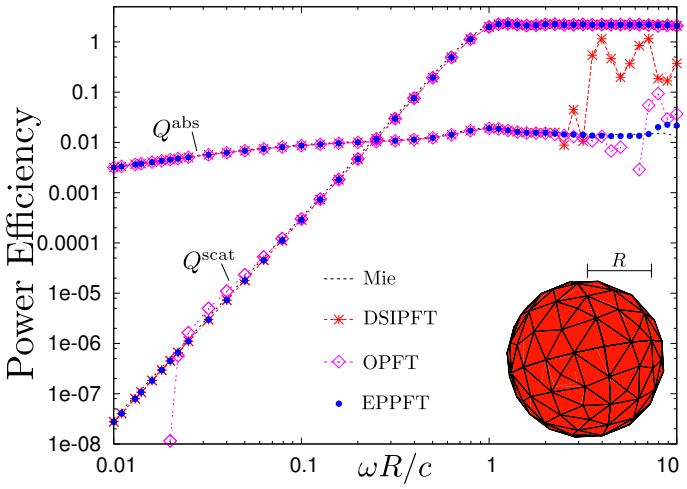

Fig. 1. Absorption and scattering efficiencies for a spherical gold nanoparticle of radius $R = 1\,\mu$m irradiated by a linearly-polarized plane wave. Efficiencies are cross sections normalized by the geometric cross section, $Q = \frac{\sigma}{\pi R^2}$. The absorption and scattering cross sections are the total absorbed and scattered power normalized by the incident power flux. Dashed lines are the predictions of Mie theory. Data points indicate calculations using the methods of this paper for a sphere discretized into $N = 206$ flat triangular panels (inset) with surface currents described by RWG basis functions.

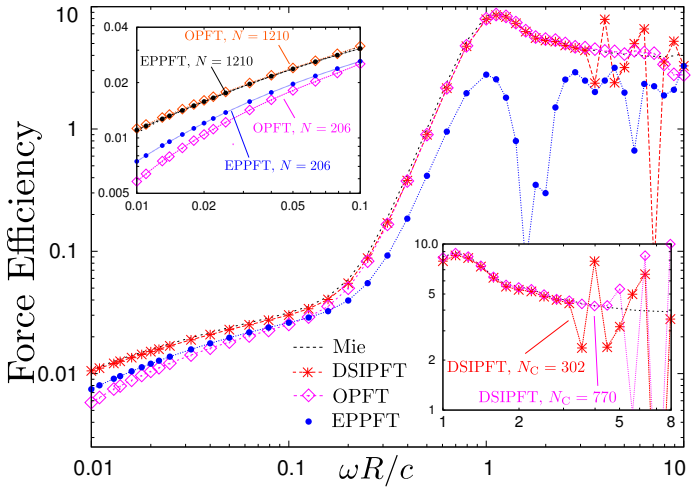

Fig. 2. Force efficiency $Q^{\rm F} = \frac{\sigma^{\rm F}}{\pi R^2}$ for the scattering problem of Figure 1. The force cross section $\sigma^{\rm F}$ is the total force on the particle divided by the incident momentum flux. *Upper inset:* For calculations of power, force, and torque (PFT) using the equivalence-principle (EPPFT) and overlap (OPFT) methods, low-frequency errors are reduced by refining the mesh discretization to $N = 1210$ panels. *Lower inset:* For calculations using the displaced-surface-integral (DSIPFT) method, high-frequency errors are reduced by refining the surface cubature rule to $N_{\rm C} = 770$ cubature points.

of cancellations from the MST integral over different parts of the body surface; the EPPFT is somewhat more accurate for the reasons discussed in the previous section. At high frequencies the EPPFT is inaccurate, due most likely to imperfect evaluation of singular integrals of the form (27). The DSIPFT is the most accurate method at low frequencies, but suffers the same high-frequency inaccuracies that are present in the power case (Figure 1) when the field oscillations over the bounding surface exceed the resolution of our fixed-order cubature method.

This article has been accepted for publication in a future issue of this journal, but has not been fully edited. Content may change prior to final publication. Citation information: DOI 10.1109/TAP.2015.2438393, IEEE Transactions on Antennas and Propagation

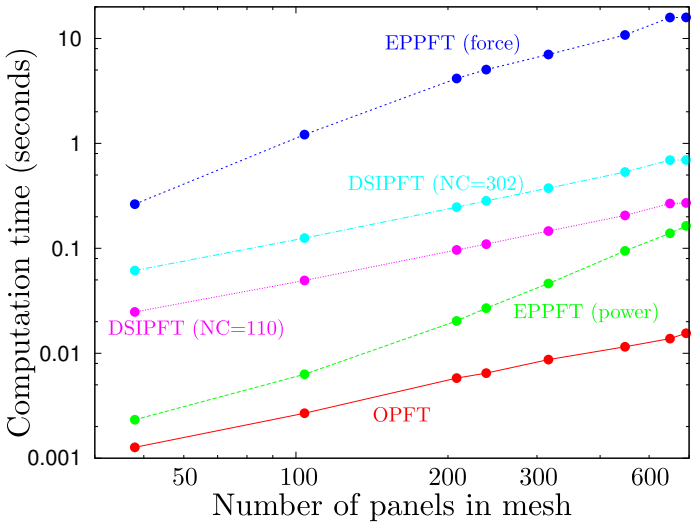

Fig. 3. Computational cost of power, force, and torque (PFT) calculations using the various algorithms presented in this paper applied to sphere meshes (like that pictured in the inset of Figure 1) with various numbers of panels. The overlap (OPFT) method is always the most efficient method, typically by several orders of magnitude.

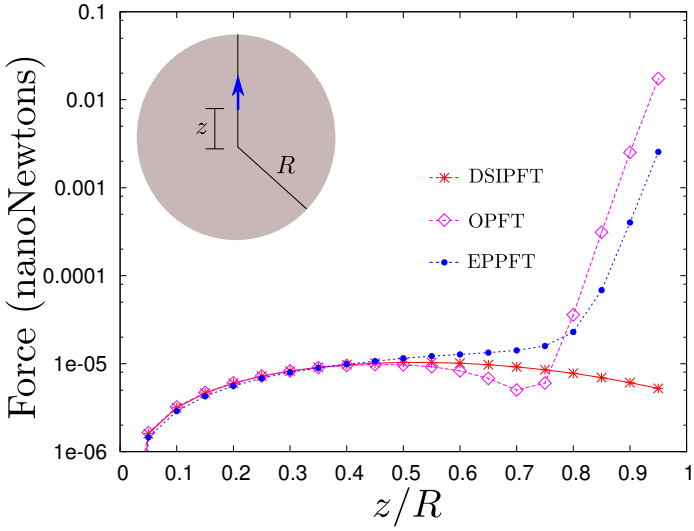

Fig. 4. z-directed force on a dielectric sphere due to a point dipole source inside the sphere. The sphere has radius 1 μm and relative dielectric constant $\epsilon^{\text{rel}} = 10$; it is discretized into a mesh like that in the inset of Figure 1, but with 924 panels. The point source is z-directed with frequency $\omega = 3 \cdot 10^{14}$ rad/sec and lies on the $\hat{z}$ axis a distance z from the center of the sphere. As the point source approaches the sphere surface ($z/R \to 1$), the overlap (OPFT) and equivalence-principle (EPPFT) calculations incur severe numerical inaccuracies, while the displaced-surface-integral (DSIPFT) calculation remains unaffected.

Comparison of computational cost.

Figure 3 plots, for sphere meshes with various total numbers of panels, the computation time required by our three methods to compute the power, force, and torque for the Mie-scattering problem of Figures 1 and 2 at the fixed frequency $\omega = 3 \cdot 10^{14}$ rad/sec. The time plotted here is only the *post-processing* time needed to compute PFTs given the surface-current vector $\mathbf{c}$; the cost of assembling and solving the linear system (11) for $\mathbf{c}$ is common to all approaches and is omitted here.

For reasons discussed above, the OPFT is always the fastest approach, typically by multiple orders of magnitude. The EPPFT calculation of the *power* is relatively fast due to the simplification noted above—namely, that the matrix elements (26) needed for the power computation in this case are already computed in assembling the BEM system (11), so their computation adds no extra time to the PFT calculation. On the other hand, the EPPFT matrices are dense, whereas the OPFT matrices are sparse, so the cost of evaluating the vector-matrix-vector products (1) is greater for EPPFT than for OPFT. DSIPFT calculations are dominated by the linear-scaling cost of evaluating the fields at the N_{C} cubature points; the figure shows the cases $N_{\text{C}} = \{110, 302\}$, with the latter incurring $3\times$ the cost of the former. Finally, the EPPFT calculation of the force and torque is the most expensive of all methods, due to the cost of evaluating the singular integrals (27).

Comparisons of computation time are of course heavily implementation-dependent, and we would not expect the precise speed ratios we found here to remain constant for other implementations. However, our computational codes [1] are implemented in C++ with significant effort invested in optimization [48], so we are confident that at least the order-of-magnitude cost ratios of Figure 3 are generally meaningful.

B. Point source inside dielectric sphere.

Figure (4) plots the z-directed force on a dielectric sphere due to a $z-$directed dipole radiator inside the sphere. The sphere has radius 1 μm and relative dielectric constant $\epsilon^{\text{rel}} = 10$ and is discretized as in the mesh inset of Figure 1, but with 924 total panels. The dipole has frequency $\omega = 3 \cdot 10^{14}$ rad/sec and is located on the positive z-axis a distance z from the sphere center. For small values of z, all three approaches yield equivalent results. However, as the dipole approaches the sphere surface ($z/R \to 1$), the OPFT and EPPFT incur severe numerical errors due to inaccurate resolution of rapidly-varying surface fields near the dipole. This problem does not affect the DSIPFT calculation, for which the fields are only evaluated on the displaced surface $\mathcal{S}$ (a sphere of radius $10R$ in this case).

In contrast to the inaccuracies exhibited by the various methods in the cases of Figures 1 and 2—which may be reduced by using finer surface meshes and surface-cubature grids—the inaccuracy exhibited by OPFT and EPPFT in the case of Figure 4 is intrinsic to this source configuration; *any* method based on PV or MST integrations over an object surface will be badly behaved as point sources approach that surface. In particular, when we calculate nonequilibrium Casimir forces and heat-transfer rates using the fluctuating-surface-current

This article has been accepted for publication in a future issue of this journal, but has not been fully edited. Content may change prior to final publication. Citation information: DOI 10.1109/TAP.2015.2438393, IEEE Transactions on Antennas and Propagation

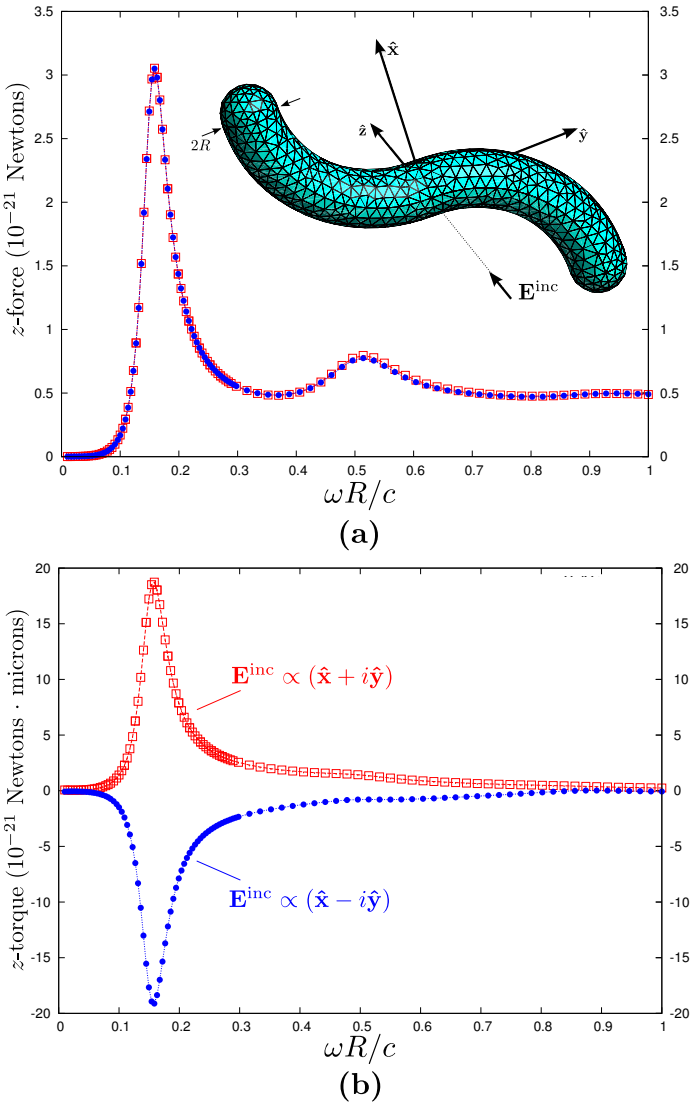

Fig. 5. z-directed force **(a)** and torque **(b)** on a chiral gold nanoparticle illuminated from below by a plane wave traveling in the positive z direction with left circular polarization (red data points) or right circular polarization (blue data points). The *force* is the same for the two incident polarizations, while the *torque* changes sign when the incident polarization is reversed.

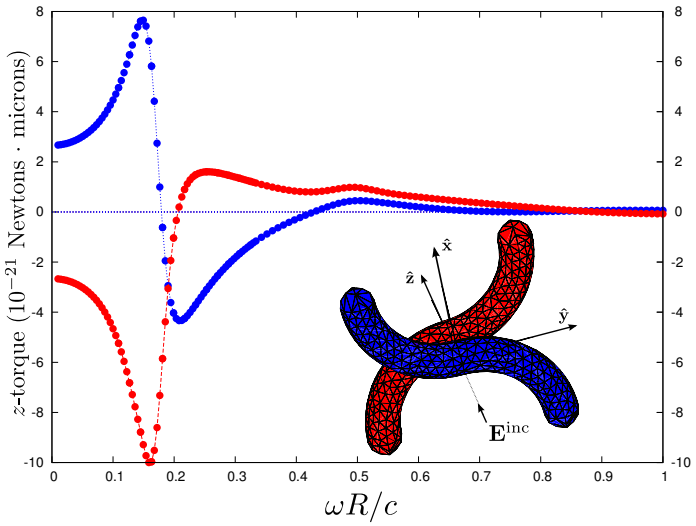

Fig. 6. z-directed torque on the lower (blue data points) and upper (red data points) members of a pair of chiral gold nanoparticles with opposite chirality separated by a surface–surface separation equal to the inner radius of the particle. The particle pair is illuminated from below by a linearly-polarized plane wave traveling in the positive z direction. Now not only the magnitudes but also the *signs* of the torques on both particles are frequency dependent, with counter-rotating and co-rotating frequency regimes.

approach [11], we effectively simulate distributions of sources lying throughout the interior of compact bodies, including at points arbitrarily close to the surface. For such problems it seems hopeless to expect accurate OPFT or EPPFT results even with high-resolution meshing; for such cases DSIPFT appears to be the only viable option.

C. Force and Torque on a Chiral Nanoparticle in a Circularly-Polarized Field

We next consider a chiral nanoparticle illuminated by a circularly-polarized plane wave. The particle is depicted in the inset of Figure 5**(a)**; it is constructed from two quarter-length sections of a torus of {inner, outer} radii $\{R, 5R\}$ (here $R = 1\mu$m) with one section rotated through π degrees and both ends capped with hemispherical endcaps. The particle is composed of gold with permittivity given by equation (38). The particle is illuminated from below by a plane wave traveling in the positive $\hat{\mathbf{z}}$ direction and either left- or right-circular polarization, i.e. we have

$$\mathbf{E}^{\text{inc}}(\mathbf{x}, t) = E_0(\hat{\mathbf{x}} \pm i\hat{\mathbf{y}})e^{i(kz-\omega t)}$$

with $k = \omega/c$ and $E_0 = 1$ V/m. Figures 5**(a)** and 5**(b)** respectively plot the force and torque on the particle as a function of frequency for both right-circularly polarized incident fields (blue circles) and left-circularly polarized incident fields (red squares). The *force* on the particle is the same for the two incident polarizations, while the *torque* changes sign when the incident polarization is reversed.

D. Frequency-Dependent Direction of Rotation on a Pair of Chiral Nanoparticles in a Linearly-Polarized Field

In the previous examples—which involved isolated nanoparticles—the PFTs could in principle have been computed by standard methods involving PV or MST integrations over distant bounding spheres surrounding the object. The methods we propose in this paper—particularly the OPFT approach—really comes into their own for geometries involving two or more closely separated bodies on which we wish separately to resolve the PFTs. In such cases, any bounding surface surrounding only one of the bodies in question must unavoidably lie close to both bodies, and the stress-tensor integral over that surface will be particularly cumbersome, whereas the OPFT technique proposed in this paper is straightforward. An example of such a geometry is provided by pairing the chiral gold nanoparticle of the previous section with a partner gold nanoparticle of opposite chirality, separated by a surface-surface separation $d = 1\,\mu$m (equal to the inner particle radius), and irradating the pair from below with a *linearly*, not circularly, polarized plane wave, $\mathbf{E}^{\text{inc}}(\mathbf{x}, \mathbf{t}) =$

This article has been accepted for publication in a future issue of this journal, but has not been fully edited. Content may change prior to final publication. Citation information: DOI 10.1109/TAP.2015.2438393, IEEE Transactions on Antennas and Propagation

$E_0\hat{\mathbf{x}}e^{i(kz-\omega t)}$. Figure 6 plots the torque on each particle, with the blue (red) data points corresponding to the lower (upper) particle. Now not only the magnitudes but also the *signs* of the torques on the two particles are frequency-dependent, with the particles either co-rotating, counter-rotating, or not rotating depending on the frequency.

IV. Conclusions

The DSIPFT formulas (13), the OPFT formulas (18), and the EPPFT formulas (24) represent three distinct ways of computing PFTs from surface currents. With exact currents and exact surface integrations, the three approaches yield equivalent results; in practical solvers—with finite basis sets and approximate surface cubatures—the three approaches lead to three numerical algorithms with differing efficiency, accuracy, and ease of implementation.

In almost all cases the OPFT formalism will be the correct choice; OPFT computations are always orders of magnitude faster than the other approaches, and (typically) equally if not more accurate. There are, however, at least two exceptions. **(1)** In cases where the extinction is dominated by absorption, such as the low-frequency tail of the scattering-efficiency curve in Figure 1, the OPFT scattered-power computation exhibits cancellation errors and is best replaced with EPPFT. **(2)** For cases involving sources inside bodies approaching the body surface (Figure 4), both OPFT and EPPFT are badly behaved and should be replaced with DSIPFT.

For an object $\mathcal{O}$ containing a volume distribution of electric current $\mathbf{J}$ in the presence of electromagnetic fields $\mathbf{E}, \mathbf{H}$, it is known [51] that the the time-average i-directed force on $\mathcal{O}$ is given by $F_i = \frac{1}{2\omega}\mathrm{Im}\int_{\mathcal{O}} \mathbf{J}^* \cdot \partial_i \mathbf{E}\, dV$, where $\partial_i \mathbf{E}$ is the derivative of $\mathbf{E}$ in the ith cartesian direction. It would be of interest to explore the consequences of this formula for equivalence-principle force and torque calculations.

In closing, we emphasize that all formulas derived in this paper are implemented in SCUFF-EM, a free, open-source software implementation of the BEM in the EFIE and PMCHWT formulations which is available for download online [1].

Acknowledgments

This work was supported in part by the Defense Advanced Research Projects Agency (DARPA) under grant N66001-09-1-2070-DOD, by the Army Research Office through the Institute for Soldier Nanotechnologies (ISN) under grant W911NF-07-D-0004, and by the AFOSR Multidisciplinary Research Program of the University Research Initiative (MURI) for Complex and Robust On-chip Nanophotonics under grant FA9550-09-1-0704.

References

[1] http://homerreid.com/scuff-EM.

[2] T. Eibert, "Some scattering results computed by surface-integral-equation and hybrid finite-element - boundary-integral techniques, accelerated by the multilevel fast multipole method," *Antennas and Propagation Magazine, IEEE*, vol. 49, no. 2, pp. 61–69, 2007.

[3] C. Uluisik, G. Cakir, M. Cakir, and L. Sevgi, "Radar cross section (rcs) modeling and simulation, part 1: a tutorial review of definitions, strategies, and canonical examples," *Antennas and Propagation Magazine, IEEE*, vol. 50, no. 1, pp. 115–126, 2008.

[4] W. L. Collett, C. A. Ventrice, and S. M. Mahajan, "Electromagnetic wave technique to determine radiation torque on micromachines driven by light," *Applied Physics Letters*, vol. 82, no. 16, pp. 2730–2732, 2003. [Online]. Available: http://link.aip.org/link/?APL/82/2730/1

[5] S. Makarov and S. Kulkarni, "Microwave radiation force and torque on a disk resonator excited by a circularly polarized plane wave," *Applied Physics Letters*, vol. 84, no. 19, pp. 3795–3797, 2004.

[6] A. Ashkin, "Acceleration and trapping of particles by radiation pressure," *Phys. Rev. Lett.*, vol. 24, pp. 156–159, Jan 1970. [Online]. Available: http://link.aps.org/doi/10.1103/PhysRevLett.24.156

[7] F. V. Ignatovich and L. Novotny, "Experimental study of nanoparticle detection by optical gradient forces," *Review of Scientific Instruments*, vol. 74, no. 12, pp. 5231–5235, 2003.

[8] W. Sun, S. Pan, and Y. Jiang, "Computation of the optical trapping force on small particles illuminated with a focused light beam using a fdtd method," *Journal of Modern Optics*, vol. 53, no. 18, pp. 2691–2700, 2006.

[9] M. Reid, A. Rodriguez, and S. Johnson, "Fluctuation-induced phenomena in nanoscale systems: Harnessing the power of noise," *Proceedings of the IEEE*, vol. 101, no. 2, pp. 531–545, 2013.

[10] M. T. Homer Reid, J. White, and S. G. Johnson, "Fluctuating Surface Currents: A New Algorithm for Efficient Prediction of Casimir Interactions among Arbitrary Materials in Arbitrary Geometries. I. Theory," *ArXiv e-prints*, Feb. 2012.

[11] A. W. Rodriguez, M. T. H. Reid, and S. G. Johnson, "Fluctuating-surface-current formulation of radiative heat transfer: Theory and applications," *Phys. Rev. B*, vol. 88, p. 054305, Aug 2013. [Online]. Available: http://link.aps.org/doi/10.1103/PhysRevB.88.054305

[12] C. F. Bohren and D. Huffman, *Absorption and scattering of light by small particles*, ser. Wiley science paperback series. Wiley, 1983. [Online]. Available: http://books.google.com/books?id=S1RCZ8BjgN0C

[13] R. Harrington, *Time-Harmonic Electromagnetic Fields*, ser. IEEE Press series on electromagnétic wave theory. IEEE Press, 1961.

[14] J. P. Barton, D. R. Alexander, and S. A. Schaub, "Internal and near-surface electromagnetic fields for a spherical particle irradiated by a focused laser beam," *Journal of Applied Physics*, vol. 64, no. 4, pp. 1632–1639, 1988. [Online]. Available: http://link.aip.org/link/?JAP/64/1632/1

[15] E. Almaas and I. Brevik, "Radiation forces on a micrometer-sized sphere in an evanescent field," *J. Opt. Soc. Am. B*, vol. 12, no. 12, pp. 2429–2438, Dec 1995. [Online]. Available: http://josab.osa.org/abstract.cfm?URI=josab-12-12-2429

[16] B. A. Kemp, T. M. Grzegorczyk, and J. A. Kong, "Optical momentum transfer to absorbing mie particles," *Phys. Rev. Lett.*, vol. 97, p. 133902, Sep 2006. [Online]. Available: http://link.aps.org/doi/10.1103/PhysRevLett.97.133902

[17] T. M. Grzegorczyk, B. A. Kemp, and J. A. Kong, "Stable optical trapping based on optical binding forces," *Phys. Rev. Lett.*, vol. 96, p. 113903, Mar 2006. [Online]. Available: http://link.aps.org/doi/10.1103/PhysRevLett.96.113903

[18] F. Xu, K. Ren, G. Gouesbet, X. Cai, and G. Gréhan, "Theoretical prediction of radiation pressure force exerted on a spheroid by an arbitrarily shaped beam," *Phys. Rev. E*, vol. 75, p. 026613, Feb 2007. [Online]. Available: http://link.aps.org/doi/10.1103/PhysRevE.75.026613

[19] K. M. Leung, "Optical bistability in the scattering and absorption of light from nonlinear microparticles," *Phys. Rev. A*, vol. 33, pp. 2461–2464, Apr 1986. [Online]. Available: http://link.aps.org/doi/10.1103/PhysRevA.33.2461

[20] L. Ng, B. Luff, M. Zervas, and J. Wilkinson, "Forces on a rayleigh particle in the cover region of a planar waveguide," *Lightwave Technology, Journal of*, vol. 18, no. 3, pp. 388–400, 2000.

[21] R. W. Going, B. L. Conover, and M. J. Escuti, "Electrostatic force and torque description of generalized spheroidal particles in optical landscapes," pp. 703 826–703 826–12, 2008.

[22] J. Chen, J. Ng, S. Liu, and Z. Lin, "Analytical calculation of axial optical force on a rayleigh particle illuminated by gaussian beams beyond the paraxial approximation," *Phys. Rev. E*, vol. 80, p. 026607, Aug 2009. [Online]. Available: http://link.aps.org/doi/10.1103/PhysRevE.80.026607

[23] Y.-X. Chen, "Radiation force of highly focused gaussian beams on a rayleigh metal particle," in *Image Analysis and Signal Processing (IASP), 2012 International Conference on*, 2012, pp. 1–5.

[24] R. Gussgard, T. Lindmo, and I. Brevik, "Calculation of the trapping force in a strongly focused laser beam," *J. Opt. Soc. Am. B*, vol. 9, no. 10, pp. 1922–1930, Oct 1992. [Online]. Available: http://josab.osa.org/abstract.cfm?URI=josab-9-10-1922

[25] R. C. Gauthier, "Ray optics model and numerical computations for the radiation pressure micromotor," *Applied Physics Letters*, vol. 67, no. 16, pp. 2269–2271, 1995. [Online]. Available: http://link.aip.org/link/?APL/67/2269/1

[26] M. Gu, D. Morrish, and P. C. Ke, "Enhancement of transverse trapping efficiency for a metallic particle using an obstructed laser beam," *Applied Physics Letters*, vol. 77, no. 1, pp. 34–36, 2000. [Online]. Available: http://link.aip.org/link/?APL/77/34/1

[27] T. A. Nieminen, V. L. Y. Loke, A. B. Stilgoe, G. Knner, A. M. Braczyk, N. R. Heckenberg, and H. Rubinsztein-Dunlop, "Optical tweezers computational toolbox," *Journal of Optics A: Pure and Applied Optics*, vol. 9, no. 8, p. S196, 2007. [Online]. Available: http://stacks.iop.org/1464-4258/9/i=8/a=S12

[28] L. Ling, F. Zhou, L. Huang, and Z.-Y. Li, "Optical forces on arbitrary shaped particles in optical tweezers," *Journal of Applied Physics*, vol. 108, no. 7, pp. 073 110–073 110–8, 2010.

[29] A. Taflove and K. Umashankar, "Review of FD-TD numerical modeling of electromagnetic wave scattering and radar cross section," *Proceedings of the IEEE*, vol. 77, no. 5, pp. 682–699, 1989.

[30] R. Dewan, I. Vasilev, V. Jovanov, and D. Knipp, "Optical enhancement and losses of pyramid textured thin-film silicon solar cells," *Journal of Applied Physics*, vol. 110, no. 1, p. 013101, 2011. [Online]. Available: http://link.aip.org/link/?JAP/110/013101/1

[31] T. Cao, L. Zhang, and M. Cryan, "Optical forces in metal/dielectric/metal fishnet metamaterials in the visible wavelength regime," *Photonics Journal, IEEE*, vol. 4, no. 5, pp. 1861–1869, 2012.

[32] L. E. McNeil, A. R. Hanuska, and R. French, "Near-field scattering from red pigment particles: Absorption and spectral dependence," *Journal of Applied Physics*, vol. 89, no. 3, pp. 1898–1906, 2001.

[33] M. Barth and O. Benson, "Manipulation of dielectric particles using photonic crystal cavities," *Applied Physics Letters*, vol. 89, no. 25, pp. 253 114–253 114–3, 2006.

[34] G. Huda and J. Hastings, "Absorption modulation of plasmon resonant nanoparticles in the presence of an afm tip," *Selected Topics in Quantum Electronics, IEEE Journal of*, vol. 19, no. 3, pp. 4 602 306–4 602 306, 2013.

[35] H.-R. Chuang, "Human operator coupling effects on radiation characteristics of a portable communication dipole antenna," *Antennas and Propagation, IEEE Transactions on*, vol. 42, no. 4, pp. 556–560, 1994.

[36] ——, "Numerical computation of fat layer effects on microwave near-field radiation to the abdomen of a full-scale human body model," *Microwave Theory and Techniques, IEEE Transactions on*, vol. 45, no. 1, pp. 118–125, 1997.

[37] W.-T. Chen and H.-R. Chuang, "Numerical computation of the em coupling between a circular loop antenna and a full-scale human-body model," *Microwave Theory and Techniques, IEEE Transactions on*, vol. 46, no. 10, pp. 1516–1520, 1998.

[38] O. Bottauscio, M. Chiampi, and L. Zilberti, "Boundary element solution of electromagnetic and bioheat equations for the simulation of sar and temperature increase in biological tissues," *Magnetics, IEEE Transactions on*, vol. 48, no. 2, pp. 691–694, 2012.

[39] A. M. Kern and O. J. F. Martin, "Surface integral formulation for 3d simulations of plasmonic and high permittivity nanostructures," *J. Opt. Soc. Am. A*, vol. 26, no. 4, pp. 732–740, Apr 2009. [Online]. Available: http://josaa.osa.org/abstract.cfm?URI=josaa-26-4-732

[40] J. J. Xiao and C. T. Chan, "Calculation of the optical force on an infinite cylinder with arbitrary cross section by the boundary element method," *J. Opt. Soc. Am. B*, vol. 25, no. 9, pp. 1553–1561, Sep 2008. [Online]. Available: http://josab.osa.org/abstract.cfm?URI=josab-25-9-1553

[41] A. Kern and O. J. F. Martin, "Pitfalls in the determination of optical cross sections from surface integral equation simulations," *Antennas and Propagation, IEEE Transactions on*, vol. 58, no. 6, pp. 2158–2161, 2010.

[42] L. N. Medgyesi-Mitschang, J. M. Putnam, and M. B. Gedera, "Generalized method of moments for three-dimensional penetrable scatterers," *J. Opt. Soc. Am. A*, vol. 11, no. 4, pp. 1383–1398, Apr 1994. [Online]. Available: http://josaa.osa.org/abstract.cfm?URI=josaa-11-4-1383

[43] S. Rao, D. Wilton, and A. Glisson, "Electromagnetic scattering by surfaces of arbitrary shape," *Antennas and Propagation, IEEE Transactions on*, vol. 30, no. 3, pp. 409–418, May 1982.

[44] L. Landau, J. Bell, J. Kearsley, L. Pitaevskii, E. Lifshitz, and J. Sykes, *Electrodynamics of Continuous Media*, ser. COURSE OF THEORETICAL PHYSICS. Elsevier Science, 1984. [Online]. Available: http://books.google.com/books?id=jedbAwAAQBAJ

[45] Y. Chen, "A mathematical formulation of the equivalence principle," *Microwave Theory and Techniques, IEEE Transactions on*, vol. 37, no. 10, pp. 1576–1581, 1989.

[46] R. Graglia, "On the numerical integration of the linear shape functions times the 3-d Green's function or its gradient on a plane triangle," *Antennas and Propagation, IEEE Transactions on*, vol. 41, no. 10, pp. 1448–1455, 1993.

[47] M. S. Tong and W. C. Chew, "On the near-interaction elements in integral equation solvers for electromagnetic scattering by three-dimensional thin objects," *Antennas and Propagation, IEEE Transactions on*, vol. 57, no. 8, pp. 2500–2506, 2009.

[48] M. T. Homer Reid, S. G. Johnson, and J. K. White, "Generalized Taylor-Duffy Method for Efficient Evaluation of Galerkin Integrals in Boundary-Element Method Computations," *ArXiv e-prints*, Dec. 2013.

[49] J. D. Jackson, *Classical Electrodynamics*, 3rd ed. John Wiley & Sons, 1999.

[50] V. Lebedev and D. N. Laikov, "A quadrature formula for the sphere of the 131st algebraic order of accuracy," *Doklady Mathematics*, vol. 59, no. 3, pp. 477–481, 1999.

[51] M. Krüger, G. Bimonte, T. Emig, and M. Kardar, "Trace formulas for nonequilibrium casimir interactions, heat radiation, and heat transfer for arbitrary objects," *Phys. Rev. B*, vol. 86, p. 115423, Sep 2012. [Online]. Available: http://link.aps.org/doi/10.1103/PhysRevB.86.115423